

## Strong Electronic Consequences of Intercalation in Cuprate Superconductors: The Case of a Trigonal Planar AuI<sub>3</sub> Complex Stabilized in the Bi<sub>2</sub>Sr<sub>2</sub>CaCu<sub>2</sub>O<sub>y</sub> Lattice

Markéta L. Munzarová<sup>†</sup> and Roald Hoffmann\*

Contribution from the Department of Chemistry and Chemical Biology, Cornell University, Ithaca, New York, 14853-1301

Received October 29, 2001

**Abstract:** Recently, a molecular AuI<sub>3</sub> complex was stabilized in the interlayer space of the Bi<sub>2</sub>Sr<sub>2</sub>CaCu<sub>2</sub>O<sub>y</sub> (Bi2212) high-*T<sub>c</sub>* superconducting phase, adopting an exceptional *D*<sub>3h</sub> structure (Choy, J.-H.; et al. *J. Phys. Chem. B* **2000**, *104*, 7273). If the gold were formally Au(III), a strong Jahn–Teller distortion to T- and Y-shaped structures would be expected. In this work, we try to understand the structural preferences of AuI<sub>3</sub> in both the gas phase and the Bi2212 lattice, as well as the influence of the AuI<sub>3</sub> intercalation on the superconductor lattice. What we think actually happens is that there is an effective electron transfer from the s-type Bi lone pair to the gold, increasing the formal oxidation state of Bi from +3 to +5 and decreasing that of Au from +3 to +1. A trigonal Au(I) trihalide is just fine. The DFT results confirm in the Bi-rich regions the same kind of electron transfer as encountered on the EHT level of theory, but they reveal additional complexities of the problem. The effect of the Bi to intercalating molecule electron transfer on the cuprate layer may be important, quite apart from this specific example, in tuning superconductivity in the cuprates.

### 1. Introduction

During the past decade, the intercalation technique has been effectively applied to the Bi<sub>2</sub>Sr<sub>2</sub>CaCu<sub>2</sub>O<sub>y</sub> superconductor (Bi2212), extending the scope of high-*T<sub>c</sub>* superconductivity (HTCS) in layered cuprates.<sup>1–6</sup>

As part of this effort, recently, a molecular AuI<sub>3</sub> complex was stabilized in the interlayer space of the Bi2212 lattice by Choy et al.<sup>7</sup> Using several spectroscopic techniques, Choy et al. concluded that a trigonal planar (*D*<sub>3h</sub>) AuI<sub>3</sub> intercalates between the two BiO layers, its plane parallel to the layer interface (see Figure 1).

Though the geometry seems on the face of it innocuous, it is rather exceptional for three-coordinated Au complexes in both solid and liquid phases.<sup>8</sup> If AuI<sub>3</sub> were neutral, the geometry is particularly surprising. AuI<sub>3</sub> is formally a d<sup>8</sup> system and as such should be Jahn–Teller unstable, with the *D*<sub>3h</sub> structure being the maximum on a typical Mexican hat-type potential energy surface. The species should have a large driving force to distort

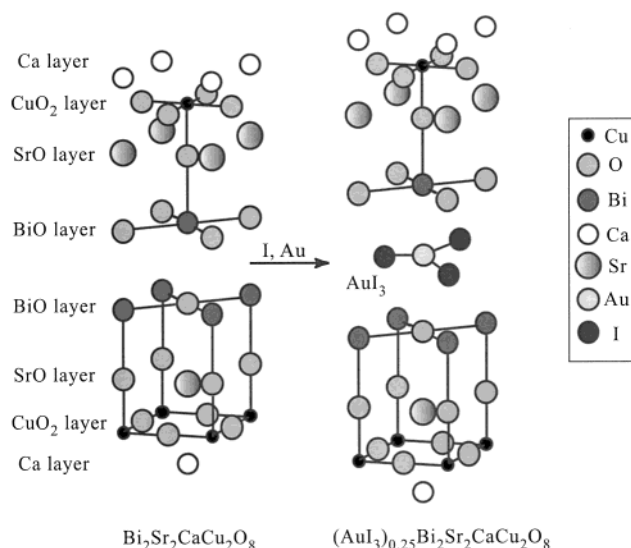


**Figure 1.** Structure of the Bi<sub>2</sub>Sr<sub>2</sub>CaCu<sub>2</sub>O<sub>y</sub> superconductor (pristine and AuI<sub>3</sub>-intercalated structures).

to *C*<sub>2v</sub> structures.<sup>9,10</sup> Recent study of AuF<sub>3</sub> and AuCl<sub>3</sub> by Hargittai et al. revealed that these two gold halides do indeed undergo a Jahn–Teller distortion to a T-shaped *C*<sub>2v</sub> structure.<sup>11,12</sup> Is there an electronic reason AuI<sub>3</sub> should behave differently?

\* To whom correspondence should be addressed. E-mail: rh34@cornell.edu.

<sup>†</sup> Present address: National Center for Biomolecular Research, Faculty of Science, Masaryk University, Kotlářská 2, CZ-611 37 Brno, Czech Republic.

- (1) Choy, J.-H.; Kwon, S.-J.; Park, G.-S. *Science* **1998**, *280*, 1589.
- (2) Choy, J.-H.; Kim, Y.-I.; Hwang, S.-J. *J. Phys. Chem. B* **1998**, *102*, 9191.
- (3) Choy, J.-H.; Hwang, S.-J.; Park, G.-S. *J. Am. Chem. Soc.* **1997**, *119*, 1624.
- (4) Choy, J.-H.; Kim, Y.-I.; Hwang, S.-J.; Yang, I.-S. *J. Solid State Chem.* **1999**, *147*, 328.
- (5) Choy, J.-H.; Hwang, S.-J.; Hwang, S.-H.; Lee, W.; Jung, D.; Lee, M.; Lee, H.-J. *J. Phys. Chem. B* **2001**, *105*, 5174.
- (6) Hwang, S.-J.; Choy, J.-H. *J. Solid State Chem.* **2001**, *160*, 39.
- (7) Choy, J.-H.; Kim, Y.-I.; Hwang, S.-J.; Huong, P. V. *J. Phys. Chem. B* **2000**, *104*, 7273.
- (8) Gimeno, M. C.; Laguna, A. *Chem. Rev.* **1997**, *97*, 511.

- (9) Albright, T. A.; Burdett, J. K.; Whangbo, M.-H. *Orbital Interactions in Chemistry*; Wiley & Sons: New York, 1985.
- (10) Komiya, S.; Albright, T. A.; Hoffmann, R.; Kochi, J. *J. Am. Chem. Soc.* **1976**, *98*, 7255.
- (11) Réffy, B.; Kolonits, M.; Schulz, A.; Klapötke, T. M.; Hargittai, M. *J. Am. Chem. Soc.* **2000**, *122*, 3127.
- (12) Hargittai, M.; Schulz, A.; Réffy, B.; Kolonits, M. *J. Am. Chem. Soc.* **2001**, *123*, 1449.

Or could it be the interaction with the Bi2212 that makes AuI<sub>3</sub> adopt this unusual geometry?

There is experimental evidence that supports the latter explanation. First, the AuI<sub>3</sub> moiety in AuI<sub>3</sub>-Bi2212 is formed at 235 °C, which is far beyond the decomposition temperature of AuI (100 °C).<sup>7</sup> This suggests that the BiO bilayer of Bi2212 interacts with AuI<sub>3</sub> strongly enough to stabilize the metastable complex, possibly in a way that favors the *D*<sub>3h</sub> structure. Second, other experiments done by Choy et al. indicate that the Bi2212 superconducting lattice behaves upon intercalation as a soft base with electron-donating character.<sup>4</sup> If this is also the case for the AuI<sub>3</sub> complex, electron donation from the lattice might so-to-speak quench the Jahn-Teller force and stabilize the complex in the *D*<sub>3h</sub> symmetry. The point is that while AuI<sub>3</sub> definitely does not want to be trigonal, AuI<sub>3</sub><sup>2-</sup> does.

While it is desirable to obtain more insight into the interactions between AuI<sub>3</sub> and Bi2212, the influence of these interactions on the electronic and geometrical structure of AuI<sub>3</sub> is not the only motivation for our study. An equally (if not more) important point is the influence of these interactions on the superconductor lattice. Charge transfer between host and guest is believed to be the main factor governing the evolution of *T*<sub>c</sub> upon intercalation.<sup>1,7</sup> Therefore, understanding such charge transfers may lead to an identification of the electronic parameters that correlate with *T*<sub>c</sub>. Though any one-electron theory that neglects many-particle interactions cannot by itself give an account of high-*T*<sub>c</sub> superconductivity, knowledge of the one-electron parameters correlated with *T*<sub>c</sub> would be of use.<sup>13</sup>

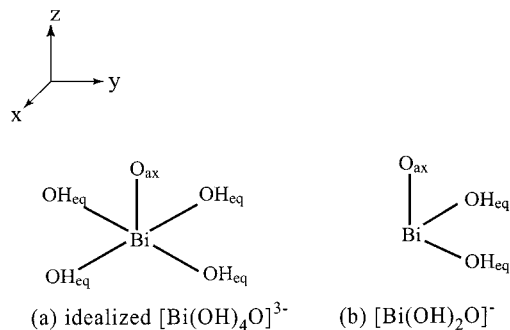
In this work, we will attempt to understand the structural preferences of AuI<sub>3</sub> in both the gas phase and the Bi2212 lattice, as well as the influence of the AuI<sub>3</sub> intercalation on the superconductor lattice. We begin with the electronic structure of *D*<sub>3h</sub> AuI<sub>3</sub> in the gas phase. Then we perform geometry optimizations to explore other important points on the potential energy surface. Finally, we study the interactions between AuI<sub>3</sub> and Bi2212, using several molecular models of the superconductor lattice. Throughout the work, a combination of extended Hückel (EHT), density functional (DFT), and second-order Møller-Plesset (MP2) methods was used.

## 2. Structural Models of the Bi2212 Lattice

The structure of the Bi2212 lattice is pseudotetragonal (*I4/mmm*), and refinements in that aristotype space group give the structure shown on the left side of Figure 1. However, the structural determination of Bi2212 is greatly complicated by stacking faults, modulations, and oxygen and cation disorder. The true symmetry of the phase is not greater than pseudo-orthorhombic; a number of space groups have been employed in an effort to describe this intractable structure.<sup>14</sup> Since the BiO layers oxygen positions are especially poorly constrained, the Bi-O ordering in Bi2212 remains to this day an open question.<sup>15</sup>

Displacements in the BiO layers appear to be a consequence of a size mismatch between CuO<sub>2</sub> and BiO layers. The Cu-O bond length in the CuO<sub>2</sub> sheets (1.91 Å) forces the average

Chart 1



Bi-O distances in the BiO layers to be 2.69 Å for the ideal structure. This distance is too long for a Bi<sup>III</sup>-O bond,<sup>16</sup> as typical bond distances in Bi<sub>2</sub>O<sub>3</sub> polyoxides are on average 2.2–2.3 Å (cf. international crystal structure database). Thus, there must occur displacements within the BiO sheet to create some shorter (and some longer) Bi-O bonds.<sup>16</sup> A number of X-ray and neutron diffraction studies,<sup>15,17–22</sup> indicate that — including the axial oxygens from the two neighboring layers — three short (2.0–2.4 Å) and three long (3.0–3.5 Å) Bi-O bonds are formed. It has been noted that a qualitatively different electronic structure of the material is obtained for these distorted structures compared to the idealized ones.<sup>21</sup>

To the best of our knowledge, the most recent study on the modulated structure of Bi2212 is that of Gladyshevskii and Flükiger,<sup>23</sup> who reported an X-ray study with a refinement in a 9-fold supercell. The authors found Bi-rich regions with distorted rock salt-type atom arrangements as well as Bi-poor regions where zigzag chains of corner-linked BiO<sub>3</sub> tetrahedra are formed. Bi atoms situated in the zigzag chains have short distances to two O atoms of the chains (2.17 and 2.30 Å) and to a third O atom, situated in the SrO layer (2.51 Å). The two next nearest O atoms are from the neighboring BiO layer at a distance of 3.26 Å.

In the present study, we adopt several molecular models of the BiO layer including the axial oxygen atom from the SrO layer and investigate these at the extended Hückel and density functional levels of theory. First, we performed calculations on the idealized rock salt-type BiO arrangement represented by the [Bi(OH)<sub>4</sub>O]<sup>3-</sup> unit (Chart 1a). The equatorial Bi-O bond lengths of 2.70 Å were adopted based on the experimental data summarized by Ginsberg,<sup>14</sup> but also shorter Bi-O<sub>eq</sub> bonds were considered, cf. below. The axial Bi-O bond length of 2.06 Å was adopted from the experimental study by Choy et al.<sup>7</sup> The second model adopted in this study is a [Bi(OH)<sub>2</sub>O]<sup>-</sup> unit with a distorted trigonal-pyramidal structure based on the results of Gladyshevskii and Flükiger, cf. Chart 1b. The equatorial Bi-O

- (13) Pavarini, E.; Dasgupta, I.; Saha-Dasgupta, T.; Jepsen, O.; Andersen, O. K. *Phys. Rev. Lett.* **2001**, *87*, 047003.  
 (14) Ginsberg, D. M. *Physical properties of high-temperature superconductors*; World Scientific: Singapore, 1989.  
 (15) Kizler, P.; Su, H. L.; Majewski, P.; Aldinger, F. *Physica C* **1994**, *233*, 415.

- (16) Torardi, C. C.; Parise, J. B.; Subramanian, A.; Gopalakrishnan, J.; Sleight, A. W. *Physica C* **1989**, *157*, 115.  
 (17) von Schnering, H. G.; Waltz, L.; Schwartz, M.; Becker, W.; Hartweg, M.; Popp, T.; Hettich, B.; Müller, P.; Kämpf, G. *Angew. Chem., Int. Ed. Engl.* **1988**, *27*, 574.  
 (18) Bordet, P.; Capponi, J. J.; Chaillout, C.; Chenavas, J.; Hewat, A. W.; Hewat, E. A.; Hodeau, J. L.; Marezio, M.; Tholence, J. L.; Tranqui, D. *Physica C* **1988**, *156*, 189.  
 (19) Sequeira, A.; Rajagopal, H.; Yakhami, J. V. *Physica C* **1989**, *157*, 515.  
 (20) Sequeira, A.; Rajagopal, H.; Nagarajan, R.; Rao, C. N. R. *Physica C* **1989**, *159*, 87.  
 (21) Ren, J.; Jung, D.; Whangbo, M.-H.; Tarascon, J.-M.; Le Page, Y.; McKinnon, W. R.; Torardi, C. C. *Physica C* **1989**, *158*, 501–506.  
 (22) Levin, A. A.; Smolin, Y. I.; Shepelev, Y. F.; *J. Phys.: Cond. Matt.* **1994**, *6*, 3539.  
 (23) Gladyshevskii, R. E.; Flükiger, R. *Acta Crystallogr.* **1996**, *B52*, 38.

Chart 2

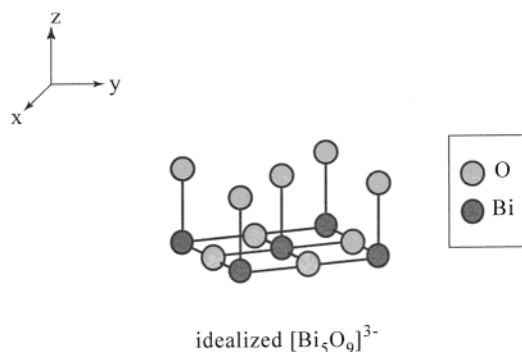
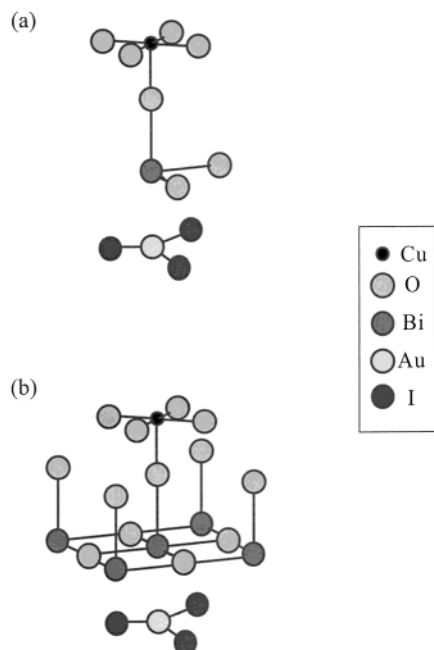


Chart 3



bond lengths were set to 2.24 Å (representing the average of 2.17 and 2.30 Å);<sup>23</sup> the axial bond length of 2.06 Å was again taken from the study by Choy et al.<sup>7</sup> For both models, the O–H bond lengths in the hydroxyl groups were fixed at 0.95 Å and the Bi–O–H angles taken as 180°.

The models selected represent the smallest chemically meaningful fragments of the corresponding extended structures. The hydrogen atoms were included in the models in order to keep the total negative charge of the systems as small as possible. (The DFT description performed for these systems in the next section would be problematic otherwise.) Also, protons attached to the oxygens may model better the electronegativity of oxygens in the extended structure.

A further model of the BiO layer, an idealized rock salt-type  $[\text{Bi}_5\text{O}_9]^{3-}$  system (Chart 2) was studied at the DFT level of theory. The model was investigated with Bi–O<sub>ax</sub> bond lengths of 2.06 Å and Bi–O<sub>eq</sub> bond lengths of, first, 2.70 Å and, second, 2.50 Å.

To explore the interaction between AuI<sub>3</sub>, the BiO and the CuO layers, two models were studied: a AuI<sub>3</sub>···[Bi(OH)<sub>2</sub>O]<sup>−</sup>···[Cu(OH)<sub>4</sub>]<sup>2−</sup> system (Chart 3a, hydrogen atoms have been for simplicity omitted), and a AuI<sub>3</sub>···[Bi<sub>5</sub>O<sub>9</sub>]<sup>3−</sup>···[Cu(OH)<sub>4</sub>]<sup>2−</sup> system (Chart 3b). The bond lengths in the Bi-containing units were chosen as stated above. AuI<sub>3</sub> was taken as a *D*<sub>3h</sub> complex

with Au–I bond lengths of 2.56 Å,<sup>7</sup> the Cu–O bond lengths were set to 1.91 Å, the O–H bond lengths 0.95 Å, and the O<sub>ax</sub>–Cu bond lengths to 2.46 Å (cf. Ginsberg<sup>14</sup>), and the Au–Bi bond length was varied as described below.

### 3. Computational Details

Extended Hückel calculations were performed using the default parameters of the CACAO program<sup>24</sup> for all atoms involved.

The single-point density functional calculations for isolated AuI<sub>3</sub> were carried out using the restricted open shell BP86 functional in both the Amsterdam density functional (ADF1999.02)<sup>25</sup> implementation and the BP86 and BHP86 functionals (cf. below) in the Gaussian98<sup>26</sup> implementation. Within the former implementation, triple- $\zeta$  STO basis sets from the ADF database were used, and the core atomic orbitals were frozen out to 4p (I) and 5p (Au). Within the latter implementation, we employed a (8s7p6d)/[6s5p3d]-GTO valence basis set for gold and a (5s5p2d)/[4s4p2d]-GTO valence basis for iodines. Small multielectron-adjusted quasirelativistic effective core potentials (ECPs) were used for both Au and I atoms. Both the basis sets and the ECPs were those of the Stuttgart group.<sup>27</sup> The geometry optimizations for AuI<sub>3</sub> were done using the BP86 and the MP2 methods in the Gaussian98 implementation only, using the same basis sets and ECPs as described above.

Computational studies of the models of the BiO layer and its interactions with AuI<sub>3</sub> and  $[\text{Cu}(\text{OH})_4]^{2-}$  were performed using the BHP86 functional in the Gaussian98 implementation. The latter, "half-and-half" hybrid functional combines Becke's generalized-gradient-correction (GGA) functional for exchange (B),<sup>28</sup> including 50% Hartree–Fock exchange (H), with Perdew's 1986 GGA<sup>29</sup> (P86) for correlation. Such functionals are somewhat less popular but perform well for certain classes of open-shell transition metal compounds,<sup>30</sup> especially those with relatively small HOMO–LUMO gaps, as is here the case for BiO layer models including  $[\text{Cu}(\text{OH})_4]^{2-}$ . Comparative calculations employing the more widely used B3LYP functional for several BiO layer models with sufficient HOMO–LUMO gaps demonstrated that both levels of theory (B3LYP and BHP86) give qualitatively the same results. We employed a (5s5p1d)/[3s3p1d]-GTO valence basis set for Bi and O, (8s7p6d)/[6s5p3d]-GTO valence basis set for Cu (both basis sets of the Stuttgart group<sup>27</sup>), and a (4s1p)/[2s1p] hydrogen basis.<sup>31</sup>

All the Bi- and Cu-containing model systems possess a total negative charge ranging from −1 through −3 to −5. In the DFT calculations,

- (24) (a) Mealli, C.; Proserpio, D. M. *J. Chem. Educ.* **1990**, *67*, 399. (b) Mealli, C.; Ienco, A.; Proserpio, D. M. *Book of Abstracts of the XXXIII ICCG*; Florence, Italy, 1998; Abstr. 510.
- (25) (a) Baerends, E. J.; Ellis, D. E.; Ros, P. *Chem. Phys.* **1973**, *2*, 41. (b) Versluis, L.; Ziegler, T. *J. Chem. Phys.* **1988**, *88*, 322. (c) te Velde, G.; Baerends, E. J. *J. Comput. Phys.* **1992**, *99*, 84. (d) Fonseca Guerra, C.; Snijders, J. G.; te Velde, G.; Baerends, E. J. *Theor. Chem. Acc.* **1998**, *99*, 391.
- (26) Frisch, M. J.; Trucks, G. W.; Schlegel, H. B.; Scuseria, G. E.; Robb, M. A.; Cheeseman, J. R.; Zakrzewski, V. G.; Montgomery, J. A., Jr.; Stratmann, R. E.; Burant, J. C.; Dapprich, S.; Millam, J. M.; Daniels, A. D.; Kudin, K. N.; Strain, M. C.; Farkas, O.; Tomasi, J.; Barone, V.; Cossi, M.; Cammi, R.; Mennucci, B.; Pomelli, C.; Adamo, C.; Clifford, S.; Ochterski, J.; Petersson, G. A.; Ayala, P. Y.; Cui, Q.; Morokuma, K.; Malick, D. K.; Rabuck, A. D.; Raghavachari, K.; Foresman, J. B.; Cioslowski, J.; Ortiz, J. V.; Stefanov, B. B.; Liu, G.; Liashenko, A.; Piskorz, P.; Komaromi, I.; Gomperts, R.; Martin, R. L.; Fox, D. J.; Keith, T.; Al-Laham, M. A.; Peng, C. Y.; Nanayakkara, A.; Gonzalez, C.; Challacombe, M.; Gill, P. M. W.; Johnson, B. G.; Chen, W.; Wong, M. W.; Andres, J. L.; Head-Gordon, M.; Replogle, E. S.; Pople, J. A. *Gaussian 98*, revision A.7; Gaussian, Inc.: Pittsburgh, PA, 1998.
- (27) (a) Dolg, M.; Wedig, U.; Stoll, H.; Preuss, H. *J. Chem. Phys.* **1987**, *86*, 866. (b) Bergner, A.; Dolg, M.; Küchle, W.; Stoll, H.; Preuss, H. *Mol. Phys.* **1993**, *80*, 1431.
- (28) Becke, A. D. *Phys. Rev. A* **1988**, *38*, 3098.
- (29) Perdew, J. P.; Wang, Y. *Phys. Rev. B* **1986**, *33*, 8822. Perdew, J. P.; Wang, Y. *Phys. Rev. B* **1986**, *34*, 7406.
- (30) Holthausen, M. C.; Heinemann, C.; Cornehl, H. H.; Koch, W.; Schwarz, H. *J. Chem. Phys.* **1995**, *102*, 4931.
- (31) Dunning, T. H.; Hay, H. In *Methods of Electronic Structure Theory*; Schaefer, H. F., III, Ed.; Modern Theoretical Chemistry; Plenum Press: New York, 1977; Vol. 3.

**Table 1.** Occupied MOs of AuI<sub>3</sub>: DFT Results<sup>a</sup>

MO <sup>b</sup>	character <sup>c</sup>	
	Au	I
4e'	6p <sub>x</sub> , 6p <sub>y</sub> 1%; 5d <sub>xy</sub> , 5d <sub>x<sup>2</sup>-y<sup>2</sup></sub> 11%	5p <sub>x</sub> , 5p <sub>y</sub> 88%
2e''	5d <sub>xz</sub> , 5d <sub>yz</sub> 4%	5p <sub>z</sub> 95%
1a <sub>2</sub> '		5p <sub>x</sub> , 5p <sub>y</sub> 100%
1a <sub>2</sub> ''	6p <sub>z</sub> 7%	5p <sub>z</sub> 93%
3e'	6p <sub>x</sub> , 6p <sub>y</sub> 10%, 5d <sub>xy</sub> , 5d <sub>x<sup>2</sup>-y<sup>2</sup></sub> 1%	5p <sub>x</sub> , 5p <sub>y</sub> 88%
3a <sub>1</sub> '	6s 23%, 5d <sub>z<sup>2</sup></sub> 22%	5p <sub>x</sub> , 5p <sub>y</sub> 56%
1e''	5d <sub>xz</sub> , 5d <sub>yz</sub> 96%	5p <sub>z</sub> 4%
2a <sub>1</sub> '	6s 1%, 5d <sub>z<sup>2</sup></sub> 74%	5s, 5p <sub>x</sub> , 5p <sub>y</sub> 24%
2e'	5d <sub>xy</sub> , 5d <sub>x<sup>2</sup>-y<sup>2</sup></sub> 81%	5s, 5p <sub>x</sub> , 5p <sub>y</sub> 18%
1e'	6p <sub>x</sub> , 6p <sub>y</sub> 4%, 5d <sub>xy</sub> , 5d <sub>x<sup>2</sup>-y<sup>2</sup></sub> 6%	5s 89%
1a <sub>1</sub> '	6s 6%, 5d <sub>z<sup>2</sup></sub> 4%	5s 91%

<sup>a</sup> MO compositions determined by MPA analysis of the BP86 (ADF) results. The order of MOs in the table corresponds to the energy level ordering (highest-lying MOs first). <sup>b</sup> This MO labeling omits the semicore iodine 4d orbitals that were included in the basis set for the DFT calculation. <sup>c</sup> In this and the following tables, orbital contributions smaller than 1% have been omitted.

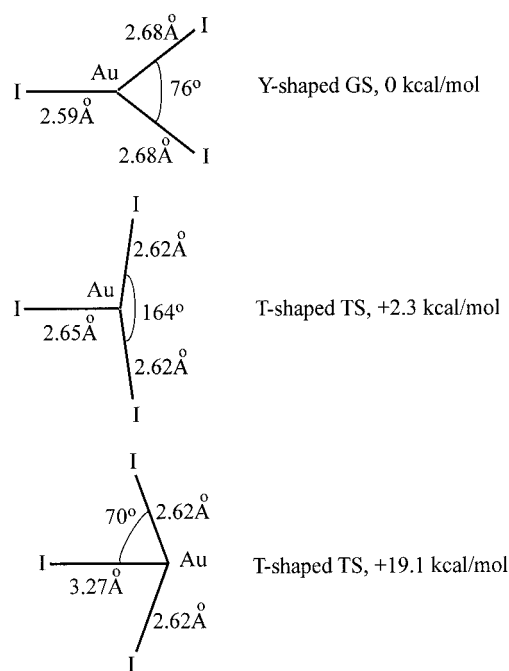
this has been consistently compensated by distributing an equivalent positive charge through a system of partial charges on the positions of the four nearest-neighbor Sr ions (in Cu-containing systems also on the four nearest-neighbor Ca sites). Introducing the partial charges results in a uniform stabilization of both occupied and virtual MOs that is approximately linearly proportional to the amount of charge applied. The electric fields that just compensate for the negative molecular charges are in all cases sufficient to make all electrons formally bound. This simple approach unfortunately then did not allow us to optimize the geometry of the intercalated AuI<sub>3</sub>, as optimization algorithms in Gaussian98 do not account for the electric field effects.

#### 4. AuI<sub>3</sub> in the Gas Phase

The *D*<sub>3h</sub> ML<sub>3</sub> system should have a d orbital splitting e'' (d<sub>xz</sub>, d<sub>yz</sub>) below a<sub>1</sub>' (d<sub>z<sup>2</sup></sub>) below e' (d<sub>xy</sub>, d<sub>x<sup>2</sup>-y<sup>2</sup></sub>), with e' doubly occupied and thus the source of Jahn–Teller instability. The actual AuI<sub>3</sub> case is complicated by the p-type lone pairs on the iodides. These in fact dominate the region near the HOMO, with the Au 5p orbitals lower in energy. Still, the results of the density functional calculations (Table 1) reveal that the doubly occupied 4e' HOMO has a substantial 5d<sub>xy</sub>, 5d<sub>x<sup>2</sup>-y<sup>2</sup></sub> contribution.<sup>32</sup> We note that the results in Table 1 refer to BP86 calculation in the ADF implementation but that the other levels of theory employed (BP86 and BHP86/Gaussian98) give very similar bonding pictures.

As a result of the orbital ordering, which is exactly as expected from qualitative considerations, there is a strong Jahn–Teller distortive force in the system. No stationary point of the AuI<sub>3</sub> potential energy surface is found unless the system is allowed to deform. A relaxation of the symmetry to *C*<sub>2v</sub> resulted in the identification of three stationary points, one minimum (ground state, GS) and two first-order saddle points (transition state, TS); see Chart 4.

The minimum corresponds to a Y-shaped structure with two larger and one smaller angles (142°, 142°, 76°) and two longer and one shorter bonds (2.68, 2.68, 2.59 Å). Both of the saddle points are T-shaped structures. The first of these lies 2.3 kcal/mol above the Y-shaped minimum, having two smaller and one larger angles (98°, 98°, 164°) and all of the bond lengths close

**Chart 4**

to each other (2.62, 2.62, 2.65 Å). The second saddle point lies 19.1 kcal/mol above the minimum, with bond angles (70°, 70°, 220°) and two short and one much longer bond lengths (2.62, 2.62, 3.27 Å).

AuI<sub>3</sub> thus offers us a typical Jahn–Teller system, characterized by a Mexican hat-type potential energy surface. The central *D*<sub>3h</sub> point is a maximum; there are Y-shaped minima and lower-lying T-shaped saddle points on the “brim” of the hat around the central maximum. The higher-lying T-shaped stationary point can probably be understood as lying on the way to dissociation of AuI<sub>3</sub> into AuI<sub>2</sub> and I<sup>-</sup>. A geometry optimization of AuI<sub>3</sub> in the triplet state restricted to the *D*<sub>3h</sub> symmetry yielded a minimum lying 5.0 kcal/mol above the singlet Y-shaped minimum, with the Au–I bond length being 2.65 Å.

Due to the dispersion energy problem, many of the currently used density functionals tend to underestimate interaction energies and overestimate bond lengths for weakly bonded complexes.<sup>33</sup> To estimate the influence of the dispersion interactions on the optimized structures and energies of AuI<sub>3</sub>, we performed geometry optimizations at the MP2 level of theory. Again, a Y-shaped structure was found to be an energy minimum, with angles (138°, 138°, 84°) and bonds on average 0.04 Å shorter than at the DFT level (2.63, 2.63, 2.56 Å). A T-shaped first-order saddle point with the angles (97°, 97°, 166°) and bond lengths (2.60, 2.60, 2.62 Å) lies only 0.2 kcal/mol above the Y-shaped minimum. Very recently, a T-shaped TS of a related AuH<sub>3</sub> system was observed stabilized in a solid matrix upon interaction with H<sub>2</sub>, which is an interesting counterpart of the AuI<sub>3</sub> stabilization reported here.<sup>34</sup>

During the preparation of the present report, studies on the electronic structure of gold iodides by Schulz and Hargittai<sup>35</sup> and by Söhnel et al.<sup>36</sup> were published. In their very careful study,

(32) For a comparison, EHT calculations on AuI<sub>3</sub> (*D*<sub>3h</sub>) were performed. The qualitative features of the electronic structure are similar for both approaches, except for the fact that the frontier orbitals 4e' and 2e'' are more covalent for EHT than for DFT and that the energies of the 1e'', 2a<sub>1</sub>' MOs are switched.

(33) Koch, W.; Holthausen, M. C. *A Chemist's Guide to Density Functional Theory*; Wiley-VCH: Weinheim, 2000.

(34) Wang, X.; Andrews, L. *J. Am. Chem. Soc.* **2001**, *123*, 12899.

(35) Schulz, A.; Hargittai, M. *Chem. Eur. J.* **2001**, *7*, 3657.

(36) Söhnel, T.; Brown, R.; Kloos, L.; Schwerdtfeger, P. *Chem. Eur. J.* **2001**, *7*, 3167.

Schulz and Hargittai<sup>35</sup> explored the PES of gold trihalides and found that a Y-shaped structure represents an energy minimum and a T-shaped structure a transition state for AuI<sub>3</sub> at the B3LYP level of theory.<sup>37</sup> Interestingly, their MP2 results suggest that even the Y-shaped structure does not appear to be a true minimum but a transition state.<sup>38</sup> This encouraged them to check the PES of AuI<sub>3</sub> beyond the Jahn–Teller surface. They found that there is indeed a L-shaped structure with C<sub>s</sub> symmetry, lying much lower in energy than both of the C<sub>2v</sub>-symmetrical stationary points.

Söhnel et al.<sup>36</sup> have drawn the same conclusions regarding the relative energies of the Y- and T-shaped structures of AuI<sub>3</sub> as found in this study and by Schulz and Hargittai, and they also studied the interaction between AuI<sub>3</sub> and Bi2212. Unfortunately, their model of the superconductor lattice appears to us inadequate, as it considers only atoms within the idealized BiO planes and disregards completely the strongly bound axial oxygen atoms (O<sub>ax</sub>; see Chart 1). As a consequence, Bi in their model is formally in the +2 oxidation state, whereas the oxidation state in the real lattice is +3. The Bi–O<sub>ax</sub> bond length is in fact significantly shorter than the average Bi–O<sub>eq</sub> bond length (2.06 vs 2.70 Å), and strong interactions with Bi orbitals should thus be expected. Indeed, O<sub>ax</sub> orbitals mix considerably into bands close to ε<sub>Fermi</sub>, as has been shown by band structure calculations (see ref 39) and as is reproduced by our molecular models (see below). It is thus not surprising that in the study of Söhnel et al. it was difficult to achieve SCF convergence—their model disregarded O<sub>ax</sub> and consequently had the wrong number of electrons.

## 5. Interaction between AuI<sub>3</sub>, the BiO, and the CuO<sub>2</sub> Layers: EHT Results

In this section, we discuss the interaction between AuI<sub>3</sub>, one of the two BiO layers, modeled by the [Bi(OH)<sub>4</sub>O]<sup>3-</sup> and the [Bi(OH)<sub>2</sub>O]<sup>-</sup> units, and the CuO<sub>2</sub> layer, modeled by the [Cu(OH)<sub>4</sub>]<sup>2-</sup> unit.

The limited gallery height for the Au–I layer within (AuI<sub>3</sub>)<sub>0.25</sub>Bi<sub>2</sub>Sr<sub>2</sub>CaCu<sub>2</sub>O<sub>y</sub> we think constrains the AuI<sub>3</sub> complex to an intercalated planar structure parallel to the basal plane.<sup>7</sup> However, the structural modulations have made it impossible so far to determine the relative orientation of the AuI<sub>3</sub> complex with respect to the Bi and O atoms constituting the BiO layer.

Our initial choice was to simply place the two fragments directly above each other, as shown in Figure 2. This figure also shows the most important orbital interactions (EHT results) for the idealized [Bi(OH)<sub>4</sub>O]<sup>3-</sup> model (hydrogen atoms have been omitted in the figure for the sake of simplicity).

The highest occupied MO of the [Bi(OH)<sub>4</sub>O]<sup>3-</sup> unit is displayed on the right side of Figure 2 (further details on the electronic structure of [Bi(OH)<sub>4</sub>O]<sup>3-</sup> are given in Table 2). It is composed mainly of the Bi 6s orbital (46%), hybridized away from O<sub>ax</sub> by a 6% admixture of the Bi 6p<sub>z</sub> orbital. This MO represents also the HOMO of the AuI<sub>3</sub>⋯[Bi(OH)<sub>4</sub>O]<sup>3-</sup> complex for the Bi–Au distance of 3.135 Å, which corresponds to the

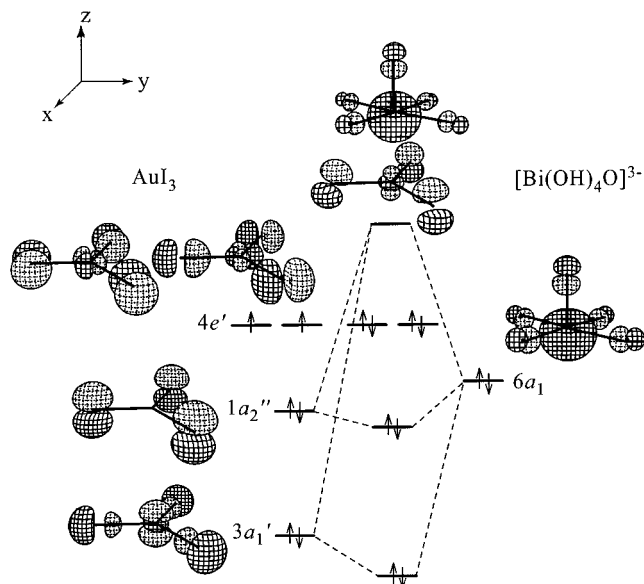


**Figure 2.** MO diagram summarizing the essential features of the interaction between AuI<sub>3</sub> and [Bi(OH)<sub>4</sub>O]<sup>3-</sup> (idealized structure).

**Table 2.** Occupied MOs of [Bi(OH)<sub>4</sub>O]<sup>3-</sup> (Idealized Structure Shown in Chart 1a): EHT Results<sup>a</sup>

MO	character			
	Bi	O <sub>eq</sub>	H <sub>eq</sub>	O <sub>ax</sub>
6a <sub>1</sub>	6s 46%, 6p <sub>z</sub> 6%	2p <sub>x,y</sub> 16%		2p <sub>z</sub> 19%
5e		2p <sub>x,y,z</sub> 82%		2p <sub>x,y</sub> 18%
1a <sub>2</sub>		2p <sub>x,y</sub> 100%		
3b <sub>1</sub>		2p <sub>z</sub> 100%		
4e		2p <sub>x,y,z</sub> 96%		2p <sub>x,y</sub> 4%
1b <sub>2</sub>		2p <sub>x,y</sub> 100%		
5a <sub>1</sub>		2p <sub>z</sub> 100%		
3e		2p <sub>x,y,z</sub> 22%		2p <sub>x,y</sub> 75%
4a <sub>1</sub>	6s 4%	2p <sub>x,y</sub> 28%		2p <sub>z</sub> 61%
2b <sub>1</sub>		2p <sub>x,y</sub> 84%	1s 12%	
2e	6p <sub>x,y</sub> 12%	2p <sub>x,y</sub> 72%	1s 14%	
3a <sub>1</sub>	6s 37%	2p <sub>x,y</sub> 40%	1s 8%	2p <sub>z</sub> 13%
2a <sub>1</sub>	6s 2%, 6p <sub>z</sub> 6%			2s 87%
1b <sub>1</sub>		2s 88%	1s 12%	
1a <sub>1</sub>		2s 84%	1s 12%	2s 4%
1e	6p <sub>x,y</sub> 2%	2s 86%	1s 12%	

<sup>a</sup> MPA analysis. The order of MOs in the table corresponds to the energy level ordering (highest-lying MOs first).

AuI<sub>3</sub> molecule being located in the middle of the BiO bilayer. As AuI<sub>3</sub> moves closer to one of the BiO layers, the repulsion experienced from the iodine-based doubly occupied orbitals pushes the HOMO of [Bi(OH)<sub>4</sub>O]<sup>3-</sup> high. At a Bi–Au distance of 2.90 Å, the repulsion is strong enough to switch the level ordering of the highest occupied MOs of AuI<sub>3</sub> and [Bi(OH)<sub>4</sub>O]<sup>3-</sup>; the doubly degenerate antibonding combination of Au 5d<sub>xy</sub>, 5d<sub>x<sup>2</sup>-y<sup>2</sup></sub> and I 5p<sub>x</sub>, 5p<sub>y</sub> accepts two electrons from the bismuth lone pair (see Figure 2). Thus, there is an effective electron transfer from the s-type Bi lone pair to the gold, increasing the formal oxidation state of Bi from +3 to +5 and decreasing that of Au from +3 to +1. The electron transfer is accompanied by a change in the electron densities of the axial oxygen of the [Bi(OH)<sub>4</sub>O]<sup>3-</sup> unit (O<sub>ax</sub>): the net Mulliken charge on O<sub>ax</sub> increases from –1.64 to –1.45.

The relative AuI<sub>3</sub>, [Bi(OH)<sub>4</sub>O]<sup>3-</sup> orientation displayed in Figure 2 represents, of course, only one of the many possible geometrical arrangements.<sup>40</sup> Any rotation of AuI<sub>3</sub> (or [Bi(OH)<sub>4</sub>O]<sup>3-</sup>) around the axis interconnecting the Au, Bi nuclei

(37) The role of the T- and Y-shaped stationary points is switched for AuF<sub>3</sub> and AuCl<sub>3</sub>: the T-shaped structure is an energy minimum whereas the Y-shaped structure is a transition state; see refs 11 and 12.

(38) The different nature of the Y-shaped stationary point suggested by our calculations as compared to ref 35 is probably caused by slightly different basis sets used and is understandable considering the very flat PES; Schulz, A., private communication.

(39) Singh, D. J.; Pickett, W. E. *J. Supercond.* **1995**, *8*, 583.

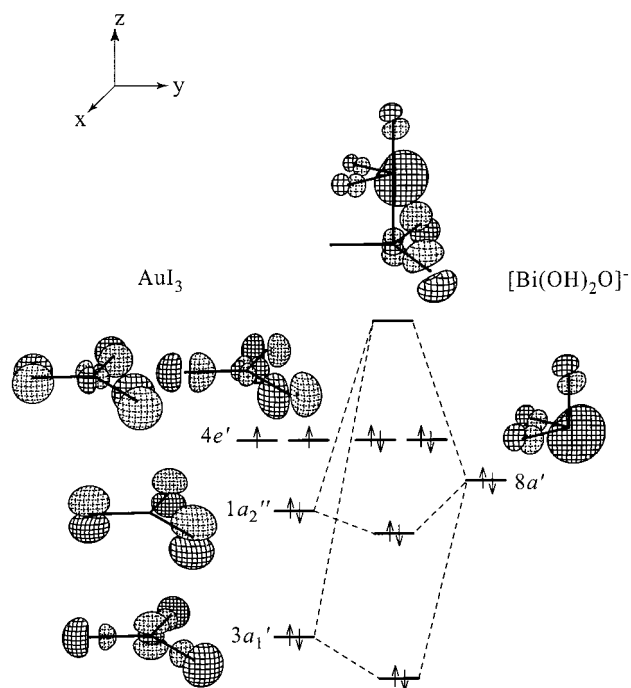


**Figure 3.** MO diagram summarizing the essential features of the interaction between  $\text{AuI}_3$  and  $[\text{Bi}(\text{OH})_2\text{O}]^-$ .

will not influence much the interactions studied in Figure 2. Disregarding the direct (through-space) interactions between the oxygens of  $[\text{Bi}(\text{OH})_4\text{O}]^{3-}$  and  $\text{AuI}_3$ , the approximate cylindrical symmetry of the Bi lone pair ensures that the overlap with the gold and the iodines is pretty much constant with respect to such a rotation. We also studied an arrangement where  $\text{AuI}_3$  was translated with respect to  $[\text{Bi}(\text{OH})_4\text{O}]^{3-}$  relative to the orientation in Figure 2 (while retaining its “parallel” orientation) so that one of the  $\text{AuI}_3$  iodines (rather than Au) was above the Bi lone pair. As expected, the repulsive interactions between the Bi lone pair and the iodines were strengthened, but followed qualitatively the same scheme as shown in Figure 2.

Let us now examine a more realistic model for the Bi environment, one with three relatively short (2.24, 2.24, 2.06 Å) Bi–O distances instead of four long and one short Bi–O contacts (see Chart 1b). Figure 3 displays the crucial orbital interactions (EHT results) between the  $[\text{Bi}(\text{OH})_2\text{O}]^-$  unit and  $\text{AuI}_3$ . (Hydrogen atoms have again been omitted in the figure for simplicity.)

The highest occupied molecular orbital of the  $[\text{Bi}(\text{OH})_2\text{O}]^-$  unit is again dominated by Bi 6s (40%), Bi 6p<sub>z</sub> (13%) contributions (for more details, see Table 3). The modified structure lowers the symmetry from  $C_{4v}$  to  $C_s$ , allowing a mixing of Bi 6p<sub>y</sub> orbital in the HOMO (15%). The Bi lone pair, as the left side of Figure 3 shows, “points” roughly along the axis of the pyramid formed by the three closer ligands. This hybridization of the HOMO strengthens (!) the interaction between the Bi lone pair and the iodines coordinated to the gold. This in turn pushes the Bi lone pair in energy above the HOMO of  $\text{AuI}_3$ , already at an Au–Bi distance of 3.0 Å. Again, the consequent electron transfer is accompanied by a change in the

(40) As pointed out by a reviewer, it would be desirable to study also the interaction of the trigonal planar and distorted  $\text{AuI}_3$  with both of the BiO layers. Though a separate study would be required to get any quantitative estimates, our EHT calculations do not suggest that any novel features would appear upon the introduction of the second BiO layer.

**Table 3.** Occupied MOs of  $[\text{Bi}(\text{OH})_2\text{O}]^-$  (Model Structure Shown in Chart 1b): EHT Results<sup>a</sup>

MO	character <sup>b</sup>			
	Bi	O <sub>eq</sub>	H <sub>eq</sub>	O <sub>ax</sub>
8a'	6s 40%, 6p <sub>y</sub> 15%, 6p <sub>z</sub> 13%	2p <sub>y</sub> 6%		2p <sub>y,z</sub> 20%
5a''		2p <sub>x,y,z</sub> 66%		2p <sub>x</sub> 32%
7a'		2p <sub>x,z</sub> 34%		2p <sub>y,z</sub> 64%
4a''		2p <sub>x,y,z</sub> 100%		
6a'		2p <sub>x,y,z</sub> 96%		2p <sub>y,z</sub> 4%
3a''		2p <sub>x,z</sub> 30%		2p <sub>x</sub> 66%
5a'	6p <sub>z</sub> 2%	2p <sub>x,y,z</sub> 60%		2p <sub>y,z</sub> 34%
4a'	6s 9%, 6p <sub>y</sub> 8%	2p <sub>x</sub> 14%		2p <sub>y,z</sub> 65%
2a''	6p <sub>x</sub> 12%	2p <sub>x,y</sub> 70%	1s 16%	
3a'	6s 28%, 6p <sub>y</sub> 8%	2p <sub>x,y</sub> 50%	1s 14%	2p <sub>z</sub> 6%
2a'	6p <sub>z</sub> 6%	2s 6%		2s 86%
1a''	6p <sub>x</sub> 3%	2s 86%	1s 12%	
1a'	6s 3%, 6p <sub>y</sub> 3%	2s 78%	1s 10%	2s 5%

<sup>a</sup> MPA analysis. The order of MOs in the table corresponds to the energy level ordering (highest-lying MOs first).

electron density of the axial oxygen of the  $[\text{Bi}(\text{OH})_2\text{O}]^-$  unit (O<sub>ax</sub>): the net Mulliken charge on O<sub>ax</sub> increases from  $-1.67$  to  $-1.51$ .

In summary, for any of the two BiO models considered, EHT predicts an effective electron transfer from the Bi lone pair to the 5d<sub>xy</sub>, 5d<sub>x<sup>2</sup>-y<sup>2</sup></sub> orbitals of gold for Au–Bi distances equal or smaller than 3.0 Å. This explains the highly unusual trigonal planar geometry of the gold triiodide, by making it formally  $\text{AuI}_3^{2-}$  with Au(I). We recently learned that Au L<sub>3</sub>-edge XANES and XPS spectroscopy carried out by the Choy group at Seoul National University points clearly to a Au(I) oxidation state in the system at hand.<sup>41</sup>

Assuming this intriguing electron transfer, how does the  $\text{AuI}_3 \cdots [\text{Bi}(\text{OH})_2\text{O}]^-$  interaction influence the electronic structure of the  $\text{CuO}_2$  plane? We model the cuprate by the  $[\text{Cu}(\text{OH})_4]^{2-}$  unit, placed as in the full structure (Chart 3a). The EHT calculations show that there are no significant interactions between the frontier orbitals of  $[\text{Bi}(\text{OH})_2\text{O}]^-$  and  $[\text{Cu}(\text{OH})_4]^{2-}$ . The latter complex is a classical d<sup>9</sup> system with a half-occupied Cu 3d<sub>x<sup>2</sup>-y<sup>2</sup></sub>-type HOMO, with substantial admixture of the OH group orbitals. The HOMO (for symmetry reasons) does not have any appreciable direct interaction with p-orbitals of the axial oxygen atom of the  $[\text{Bi}(\text{OH})_2\text{O}]^-$  group. The doubly occupied Cu 3d-centered MOs that possess symmetry-related counterparts on the O<sub>ax</sub> of  $[\text{Bi}(\text{OH})_2\text{O}]^-$  (Cu 3d<sub>xz</sub>, Cu 3d<sub>yz</sub>, Cu 3d<sub>z<sup>2</sup></sub>) do not enter any appreciable orbital interactions either.<sup>42</sup>

However, when the  $\text{AuI}_3$  component is included, an electron transfer from the Bi lone pair to the 5d<sub>xy</sub>, 5d<sub>x<sup>2</sup>-y<sup>2</sup></sub> orbitals of gold empties the HOMO of  $[\text{Bi}(\text{OH})_2\text{O}]^-$ . This in turn can accept the single electron from the HOMO of  $[\text{Cu}(\text{OH})_4]^{2-}$ . We do not trust EHT calculations to get that secondary electron transfer right; the Bi and Cu levels will shift with charge in ways that EHT may not capture. However, it seems clear that the intercalation of  $\text{AuI}_3$  in the interlayer space of the BiO bilayer in Bi2212 will increase the hole concentration within the  $\text{CuO}_2$  layer. The latter effect is also predicted by our density functional calculations on a related model (see section 6). The electron transfers between the  $\text{AuI}_3$ ,  $[\text{Bi}(\text{OH})_2\text{O}]^-$ , and  $[\text{Cu}(\text{OH})_4]^{2-}$  units are rather straightforwardly reflected in the

(41) Choy, J.-H., private communication.

(42) The maximal energy (de)stabilizations resulting from the orbital interactions encountered are  $\sim 0.1$  eV.

**Table 4.** Occupied MOs of  $[\text{Bi}(\text{OH})_2\text{O}]^-$  (Model Structure in Chart 1b): DFT Results<sup>a</sup>

MO	character <sup>b</sup>			
	Bi	O <sub>eq</sub>	H <sub>eq</sub>	O <sub>ax</sub>
5a''		2p <sub>x,z</sub> 59%		2p <sub>z</sub> 40%
8a'	6p <sub>y</sub> 4%	2p <sub>x,y,z</sub> 61%		2p <sub>x</sub> 31%
7a'	6s 3%, 6p <sub>x</sub> 5%	2p <sub>x,z</sub> 11%		2p <sub>y</sub> 77%
4a''	6p <sub>z</sub> 4%	2p <sub>x,y,z</sub> 93%		2p <sub>z</sub> 3%
6a'	6p <sub>z</sub> 2%	2p <sub>x,y,z</sub> 90%		2p <sub>y</sub> 4%
3a''	6p <sub>z</sub> 4%	2p <sub>x,z</sub> 41%		2p <sub>z</sub> 51%
5a'	6p <sub>x,y</sub> 25%	2p <sub>x,y</sub> 33%		2p <sub>x</sub> 38%
4a'	6s 16%, 6p <sub>x,y</sub> 15%	2s, 2p <sub>x,y,z</sub> 50%	1s 12%	2p <sub>y</sub> 4%
2a''	6p <sub>z</sub> 9%	2s, 2p <sub>x,y,z</sub> 71%	1s 17%	
3a'	6s 74%	2p <sub>x,y</sub> 16%	1s 5%	2s 3%
2a'	6s 3%, 6p <sub>x</sub> 1%	2s, 2p <sub>x,y</sub> 6%		2s 90%
1a''		2s 86%	1s 12%	
1a'	6s 3%	2s 81%	1s 10%	2s 4%

<sup>a</sup> MPA analysis of BHP86 results. The order of MOs in the table corresponds to the energy level ordering (highest-lying MOs first).

Mulliken charge of the O<sub>ax</sub> atom. In isolated  $[\text{Bi}(\text{OH})_2\text{O}]^-$ , the charge of O<sub>ax</sub> is  $-1.67$ ; it increases to  $-1.64$  upon the interaction with  $[\text{Cu}(\text{OH})_4]^{2-}$  and then increases further to  $-1.56$  upon the subsequent interaction with Au<sub>3</sub>. Our findings are in agreement with the results of XANES spectroscopic studies on Bi2212; these revealed partial oxidations of BiO and CuO<sub>2</sub> layers upon AgI<sub>w</sub> and HgX<sub>2</sub> intercalation.<sup>2,3,6</sup> More importantly, considering that all Bi2212 samples in ref 7 were in the slightly overdoped region of the phase diagram,<sup>41</sup> our results are fully consistent with a decrease in  $T_c$  upon the intercalation.<sup>7,43</sup>

## 6. Interaction between Au<sub>3</sub>, the BiO, and the CuO<sub>2</sub> Layers: DFT Results

DFT calculations with the hybrid BHP86 functional have also been performed for both the idealized  $[\text{Bi}(\text{OH})_4\text{O}]^{3-}$  and the more realistic  $[\text{Bi}(\text{OH})_2\text{O}]^-$  models (Chart 1). A brief inspection of the DFT results for  $[\text{Bi}(\text{OH})_2\text{O}]^-$  (Table 4) reveals that the relative ordering of the MOs is qualitatively different from that obtained at the EHT level of theory. The highest-lying occupied MOs correspond to the lone pairs of the oxygen atoms, leaving the Bi sp-hybrid lone pair at a relatively low energy. The same result was obtained for idealized  $[\text{Bi}(\text{OH})_4\text{O}]^{3-}$ , both within our nonrelativistic treatment<sup>44</sup> and when relativistic effects were explicitly accounted for.<sup>45</sup>

The qualitative disagreement between the chemically intuitive electronic structure supported by the EHT results on one side and the DFT results on the other side is unusual. Which of these descriptions is closer to reality? On one hand, one might argue that the positive charge on the Bi atom (surrounded by very electronegative ligands) — not accounted for within the EHT approach — pulls the Bi 6s orbital down in energy, the latter effect being magnified by the relativistic s-orbital contraction. On the other hand, the EHT description may suffer less from the broken boundary conditions (i.e., carving a molecular model out of the solid) when working with a molecular model.

The latter point of view is supported by the results of DFT calculations on the related BiF<sub>3</sub> system (with inclusion of relativistic effects). These predict a significant Bi 6s contribution

to the HOMO.<sup>46</sup> Furthermore, there is some experimental and theoretical evidence for the BiO double layer itself that suggests significant Bi 6s mixing in the valence band. First, several intercalation experiments showed that the BiO double layer behaves as a soft base with electron-donating character.<sup>47</sup> Second, valence band photoemission spectra of Bi2212 obtained by Fujimori et al. suggested a significant shift of the Bi 6s contribution from the deep-lying Bi 6s — O 2p bonding states to the antibonding states in the O 2p band region, as compared to the results of band structure calculations. The authors concluded that the exact oxygen content in Bi<sub>2</sub>Sr<sub>2</sub>CaCu<sub>2</sub>O<sub>y</sub> was greater than that assumed in the band structure calculations ( $y = 8$ ) and that the excess oxygens are coordinated to Bi, resulting in the upward shift of the Bi 6s level. Indeed,  $y \approx 8.25 \pm 0.1$  has been obtained from thermogravimetry.<sup>48</sup> A similar conclusion (extra oxygen coordinating to Bi may raise Bi 6s in energy so that the latter orbital provides an important contribution to the valence band spectra) was drawn from the experimental study on the Bi2201 system of Xu et al.<sup>49</sup> Last, significant Bi character of the Bi—O bands close to  $\epsilon_{\text{Fermi}}$  of Bi2201 was suggested in theoretical studies due to Singh and Pickett<sup>39</sup> and Strange and Gunn.<sup>50</sup>

This body of evidence suggests that the models with Bi coordinated by four loosely bound OH groups (idealized structure) or two more tightly bound OH groups (more realistic structure) may not represent the electronic structure of the BiO plane at the DFT level of theory well. We see two possible reasons for this. First, the oxygen atoms in the BiO plane are bound each to four electropositive Bi atoms; they are thus less electronegative than in our model, where oxygen atoms are parts of the OH groups. The less electronegative ligands are then supposed to withdraw less charge from the Bi atoms and to pull them down in energy to a smaller extent. Second, the bismuths are in reality likely to be more closely coordinated by oxygen atoms than represented by our models. Both the extra oxygen atoms (see above) and the structural modulations (Bi-rich regions<sup>23</sup>) may significantly shorten typical Bi—O bond distances.

Our density functional calculations reveal that a distant coordination of Bi by electronegative oxygens pulls Bi orbitals down in energy (electronegativity effect), whereas a close coordination pushes Bi orbitals up in energy (orbital interaction effect). For the idealized  $[\text{Bi}(\text{OH})_4\text{O}]^{3-}$  model with “average” Bi—O bond lengths of 2.7 Å, the 10 highest-lying orbitals are 85–90% composed of oxygen orbitals. Decreasing the Bi—O bond lengths from 2.7 to 2.0 Å makes the Bi 6s orbital the HOMO.<sup>51</sup>

The second step toward a more realistic model we took was to obtain a better account of the electronegativity of the oxygens surrounding the Bi atom in question. We do this considering a  $[\text{Bi}_5\text{O}_9]^{3-}$  model that corresponds to a 4-fold unit cell of the idealized BiO structure (Chart 2). Embedding of the oxygen

(43) It should be kept in mind, though, that the decrease of  $T_c$  can be more directly connected to the interaction between the CuO<sub>2</sub> plane and O<sub>ax</sub> and that structural defects may participate in  $T_c$  evolution upon intercalation.  
 (44) Note, however, that relativistic pseudopotentials have been employed.  
 (45) Rösch, N., private communication.

(46) Schwerdtfeger, P.; Boyd, P. D. W.; Fischer, T.; Hunt, P.; Liddell, M. J. *Am. Chem. Soc.* **1994**, *116*, 9620.  
 (47) See: Reference 4 and references given therein.  
 (48) Fujimori, A.; Takekawa, S.; Takayama-Muromachi, E.; Uchida, Y.; Ono, A.; Takahashi, T.; Okabe, Y.; Katayama-Yoshida, H. *Phys. Rev. B* **1989**, *39*, 2255.  
 (49) Xu, G.; Mao, Z.; Yan, H.; Liu, X.; Xu, C.; Zhang, Y. *Supercond. Sci. Technol.* **1998**, *11*, 474.  
 (50) See: Strange, P.; Gunn, J. M. F. *J. Phys.: Cond. Matt.* **1989**, *1*, 6843 and references given therein.  
 (51) Munzarová, M. L.; Hoffmann, R., unpublished results.

atoms between the four outer bismuth atoms changes radically the relative ordering of the oxygen and central bismuth energy levels. For the  $[\text{Bi}_5\text{O}_9]^{3-}$  model with in-plane Bi–O bond lengths of 2.7 Å, the HOMO contains 20% of a Bi sp-hybrid orbital. This should be compared to the HOMO of the  $[\text{Bi}(\text{OH})_4\text{O}]^{3-}$  model with the same Bi–O bond lengths that is composed exclusively of oxygen lone pairs. Experiments by Gladyshevskii and Flükiger indicate that regular Bi–O square nets are formed in Bi-rich regions in which the in-plane Bi–O bond lengths are shorter than 2.7 Å.<sup>23</sup> We therefore carried out DFT calculations for the  $[\text{Bi}_5\text{O}_9]^{3-}$  model with the in-plane Bi–O bond lengths shortened to 2.5 Å. For the latter model, the HOMO contains as much as 37% of Bi sp-hybrid orbital. Thus, diminution of the in-plane Bi–O bond lengths by 0.2 Å almost doubles the content of the Bi orbitals in the HOMO (!).

In the bismuth-poor regions of the BiO layer, zigzag chains are expected to replace the regular square net of Bi and O atoms. The  $[\text{Bi}(\text{OH})_2\text{O}]^-$  system discussed above can be considered as a minimal model of the BiO zigzag chain. Although the HOMO of the  $[\text{Bi}(\text{OH})_2\text{O}]^-$  model studied here corresponds to oxygen lone pairs (Table 4), further modulations of the bond lengths (shorter contacts within and between the chains) as well as extra oxygen insertions<sup>23</sup> are again likely to push Bi orbitals higher in energy.

Going back to the  $[\text{Bi}_5\text{O}_9]^{3-}$  model, it is of a great interest to investigate its interactions with the  $[\text{Cu}(\text{OH})_4]^{2-}$  model and the  $\text{AuI}_3$  complex at the DFT level of theory. The structural model employed for this investigation is shown at Chart 3b. Our calculations for the isolated  $[\text{Bi}_5\text{O}_9]^{3-}$  model with in-plane Bi–O bond lengths of 2.5 Å revealed the following (Mulliken) charge distribution:  $\text{Bi}_{\text{inner}} +1.20$ ,  $\text{O}_{\text{ax,inner}} -1.24$ ,  $\text{O}_{\text{eq}} -1.02$ ,  $\text{Bi}_{\text{outer}} +1.32$ , and  $\text{O}_{\text{ax,outer}} -1.04$ . Upon the interaction with the  $[\text{Cu}(\text{OH})_4]^{2-}$  unit, the charge distribution on  $\text{O}_{\text{eq}}$ ,  $\text{Bi}_{\text{outer}}$ , and  $\text{O}_{\text{ax,outer}}$  is affected only in a minor way, whereas the charge distribution between  $\text{Bi}_{\text{inner}}$  and  $\text{O}_{\text{ax,inner}}$  is modified strongly: Bi charge decreases to +0.50 and that of oxygen atoms increases to –0.50. The analysis of the spin density distribution assigns ~90% of the unpaired electron to the Cu atom, the remaining ~10% is delocalized onto the four OH groups. Finally, when the  $[\text{Bi}_5\text{O}_9]^{3-}$ ,  $[\text{Cu}(\text{OH})_4]^{2-}$  complexes interact with the  $\text{AuI}_3$  complex (3.0 Å from the BiO layer), gold triiodide accepts a total of  $0.4e^-$ , approximately equally distributed between the

four constituent atoms. About half of this redox equivalent is transferred from the  $[\text{Cu}(\text{OH})_4]^{2-}$  unit and the other half from the  $[\text{Bi}_5\text{O}_9]^{3-}$  unit. Our density functional calculations thus suggest that  $\text{AuI}_3$  intercalation results in an increase of the hole density within the  $\text{CuO}_2$  plane.

## 7. Conclusions

The present study has not only shed light on the electronic consequences of the  $\text{AuI}_3$  intercalation of the Bi2212 superconductor but also illustrated important aspects of the EHT and DFT descriptions of molecular models of extended structures. Our EHT calculations suggest that there is an effective electron transfer from the s-type Bi lone pair to the gold, increasing the formal oxidation state of Bi from +3 to +5 and decreasing that of Au from +3 to +1. Thus, a trigonal symmetry intercalate (formally  $\text{AuI}_3^{2-}$ ) is reasonable. DFT calculations predict in the Bi-rich regions the same kind of electron transfer as encountered on the EHT level of theory. Our exploration of various molecular models for the system revealed an instructive disagreement between the DFT and the EHT results, which motivated us to look more carefully at what DFT theory does in these systems. Interesting effects of the bond lengths between the bismuth atom and the surrounding oxygens, as well as of the electronegativity of the latter on the Bi energy levels, have been uncovered. The electronic structure of models of the BiO layer is very sensitive to their detailed geometry. Further experimental work on the structure of the BiO layer thus seems to be crucial for developing a detailed understanding of the *c*-axis electron transfers in Bi-containing intercalated cuprate superconductors.

**Acknowledgment.** We thank to Drs. Martin Kaupp (Würzburg), Dominik Munzar (Brno), Jin-Ho Choy and Sung Hong (Seoul), Magdolna Hargittai (Budapest), Notker Rösch and Axel Schülz (Munich), and Christian Bernhard (Stuttgart) for helpful discussions, and Peter Schwerdtfeger (Auckland) for communication of his work to us prior to publication. M.L.M. gratefully acknowledges financial support from the J. W. Fulbright Foundation. The research at Cornell was supported by the National Science Foundation through Grant CHE-99-70089.

JA012449D